



HAL
open science

Design and simulation of a 390GHz seventh harmonic gyrotron using a large orbit electron beam

Fengping Li, Wenlong He, Adrian W Cross, Craig R Donaldson, Liang Zhang, Alan D R Phelps, Kevin Ronald

► **To cite this version:**

Fengping Li, Wenlong He, Adrian W Cross, Craig R Donaldson, Liang Zhang, et al.. Design and simulation of a 390GHz seventh harmonic gyrotron using a large orbit electron beam. *Journal of Physics D: Applied Physics*, 2010, 43 (15), pp.155204. 10.1088/0022-3727/43/15/155204 . hal-00629946

HAL Id: hal-00629946

<https://hal.science/hal-00629946>

Submitted on 7 Oct 2011

HAL is a multi-disciplinary open access archive for the deposit and dissemination of scientific research documents, whether they are published or not. The documents may come from teaching and research institutions in France or abroad, or from public or private research centers.

L'archive ouverte pluridisciplinaire **HAL**, est destinée au dépôt et à la diffusion de documents scientifiques de niveau recherche, publiés ou non, émanant des établissements d'enseignement et de recherche français ou étrangers, des laboratoires publics ou privés.

Design and Simulation of a ~390 GHz 7th Harmonic Gyrotron using a large orbit electron beam

Fengping Li, Wenlong He, Adrian W. Cross, Craig R. Donaldson, Liang Zhang, Alan D. R. Phelps, and Kevin Ronald

SUPA, Department of Physics, University of Strathclyde, Glasgow, G4 0NG, United Kingdom.

E-mail: Fengping.li@strath.ac.uk

Abstract. A ~390 GHz harmonic gyrotron based on a cusp electron gun has been designed and numerically modelled. The gyrotron **operates** at the 7th harmonic of the electron cyclotron frequency with the beam interacting with a TE₇₁ waveguide mode. Theoretical as well as numerical simulation results using the 3D Particle-In-Cell (PIC) code MAGIC are presented. The cusp gun generated an axis-encircling, annular shaped electron beam of energy 40 keV, current 1.5 A with a velocity ratio α of 3. Smooth cylindrical waveguides have been studied as the interaction cavities and their cavity Q optimized for 390 GHz operation. In the simulations ~ 600 W of output power at the design frequency has been demonstrated.

Keywords: Harmonic gyrotron, terahertz, large orbit electron beam

1. Introduction:

Microwave radiation sources are one of the crucial technologies for modern society. High power sub-millimeter wave sources have attracted significant interest recently due to their potential applications in electron cyclotron resonance heating [1], plasma diagnostics [2], space radar systems [3], communication systems [4], materials science and medical imaging and spectroscopy [5,6].

The gyrotron is well known as a coherent millimeter wave source capable of high power and high frequency output which is extendable to the Terahertz (THz) frequency region. Recently a gyrotron achieved kilowatts of output power operated at the fundamental electron cyclotron frequency of 1 THz [7] by using a pulsed solenoid. However, continuous wave (CW) operation at such a frequency is a formidable task because of the large magnetic field (~ 40 T) that is required. As the output frequency increases, both larger magnetic fields and reduced interaction region size are needed when operating at the fundamental cyclotron frequency. An alternative approach to generate CW high frequency radiation is to work at higher cyclotron harmonics [8,9,10,11] which allow the use of larger cavity sizes and smaller magnetic fields by a factor of s , where s is the harmonic number.

A CW high harmonic gyrotron operating at a frequency of ~ 390 GHz at relatively lower B-field was designed and is presented in this paper. In this gyrotron cyclotron resonance takes place between the seventh harmonic of the electron cyclotron frequency ($s = 7$) and the TE_{71} waveguide mode. A large orbit electron beam from a cusp gun is used to reduce the possibility of parasitic interactions. The small-signal theory of the beam-wave interaction was used to calculate the growth rate and the starting current. A smooth-bore cavity was designed with a suitable Q value by optimizing the angle of the output taper and the length of the cavity so that the starting current requirement is met. Finally, the beam-wave interaction of the gyrotron was simulated using the 3D Particle-In-Cell (PIC) code MAGIC and the results are presented.

2. Cusp electron gun

While operating at harmonics, undesired mode competition as well as parasitic oscillations will be more problematic as the harmonic number increases, therefore, it is advantageous for an electron gun to be able to generate a mode-selective beam. A large orbit electron beam from a cusp gun was selected because for such a beam its harmonic of the cyclotron mode (s) only interacts with a TE_{mn} waveguide mode (m and n are azimuthal and radial mode index respectively) when $s = m$ [12]. A cusp electron gun operates by an electron beam passing through a non-adiabatic magnetic field reversal from negative to positive sign.

Invariance of the magnetic moment results in a large orbit, annular electron beam [13, 14, 15].

Several successful terahertz range large orbit harmonic gyrotrons experiments have been carried out at resonant magnetic fields 10.5 - 14 T [16, 17].

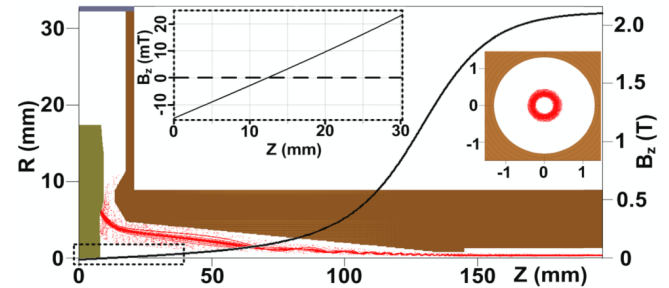


Figure 1. Simulated cusp gun and resultant beam trajectories with the detailed magnetic field configuration at the cusp point.

The 3D PIC code MAGIC was used to simulate and optimize the design of the cusp electron beam source. The optimized geometry of the cusp gun including magnetic field profile and the resultant beam trajectories are shown in figure 1. An insertion shows in detail the B-field reversal in the cusp region.

The B-field profile of the cusp was produced by two coils, a main coil and a reverse coil. The main coil produces a uniform magnetic field at the downstream region which should have a certain length of the flat-top region required by the beam-wave interaction in the cavity. Two extra layers of coils were added to both ends of the main solenoid to sharpen its B-field profile so that the overall turns and length of the solenoid were reduced. These extra coils were carefully designed to avoid any bumps in the magnetic field profile while minimizing the rise and fall distance of the magnetic field. The design parameters were optimized resulting in the production of a 40 kV, 1.5 A large orbit electron beam in the simulations. This electron beam has been optimized through adjustment of the magnetic coil arrangement to operate at a velocity ratio α from 1.2-3 [18, 19] with an inner radius of 0.27 mm and an outer radius of 0.36 mm. This is consistent with the analytical calculated Larmor radius of 0.31 mm. The reflected electrons in figure 1 are low energy electrons emitted during the rise-time of the applied voltage pulse. A velocity pitch α spread of $\sim 25\%$ was simulated when α reaches 3. Further increase of the beam α would result in a significant increase of beam spread in α hence the reflection of some beam electrons.

3. Gyrotron design

Gyrotrons are based on the CRM (Cyclotron Resonance Maser) [20] instability and operate through a fast cyclotron wave interaction, which takes place near the frequency cut-off region of the waveguide mode. In a high harmonic gyrotron, the beam (harmonic number $s > 1$) interacts with a high order TE_{mn} waveguide mode where $m = s$.

All the possible interactions are shown in figure 2. When the 7th harmonic of the electron cyclotron frequency is in resonance with the TE₇₁ mode, interactions below this mode are eliminated because the corresponding harmonic beam lines are far below their corresponding TE_{m1} waveguide mode curves except for the case of the TE₆₁ mode and $s = 6$. The other possible parasitic interactions might be from higher modes, i.e., TE₈₁ with $s = 8$ and TE₉₁ with $s = 9$, etc. However the most dangerous one is with the neighboring TE₈₁ interaction as the starting current increases as the mode index increases. But the TE₈₁ interaction has a starting current higher than the beam current. In this way any other parasitic interactions of higher modes are automatically eliminated.

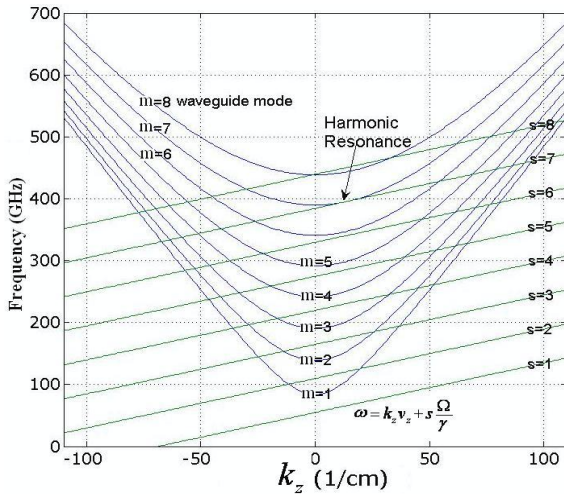


Figure 2. Dispersion of the TE_{m1} waveguide modes ($m = 1-8$) and beam-wave resonances at different harmonics.

As the gyrotron works near the cut-off frequency region, and a large orbit gyrotron requires $s = m$, the operating frequency (390 GHz) and harmonic number ($s = 7$) as well as the azimuthal index of the waveguide mode ($m = 7$) were chosen prior to the cavity size.

The interaction of the waveguide mode and axis-encircling electron beam cyclotron mode can be described by the equation below [21, 22]:

$$\omega^2 - k_z^2 c^2 = - \frac{4\beta_{\perp}^2}{(x_{mn}^2 - m^2)(\omega - k_z v_z - s\Omega)^2} \left(\frac{I}{I_A} \right) \left(\frac{x_{mn} c}{r_w} \right)^4 \left(\frac{J'_m(x_{mn} r_L / r_w)}{J_m(x_{mn})} \right)^2 \quad (1)$$

Where k_z is the propagation constant; x_{mn} is the n th root of $J'_m(x) = 0$. r_w is the radius of the cylindrical cavity; N_e is the axial linear density of electrons. $\gamma_0 = 1 + eV/m_0 c^2$ is the relativistic Lorentz factor; m_0 is the rest mass of an electron, V is electron beam voltage. $\beta_{\perp} = v_{\perp}/c$; $r_L = v_{\perp}/\Omega$ is the electron Larmor radius. $\Omega = eB/\gamma_0 m_0$ is the electron gyrating frequency, where B is the magnetic field. I is the beam current and $I_A = 4\pi\epsilon_0 m_0 c^3 / e \approx 17$ kA is the Alfvén current.

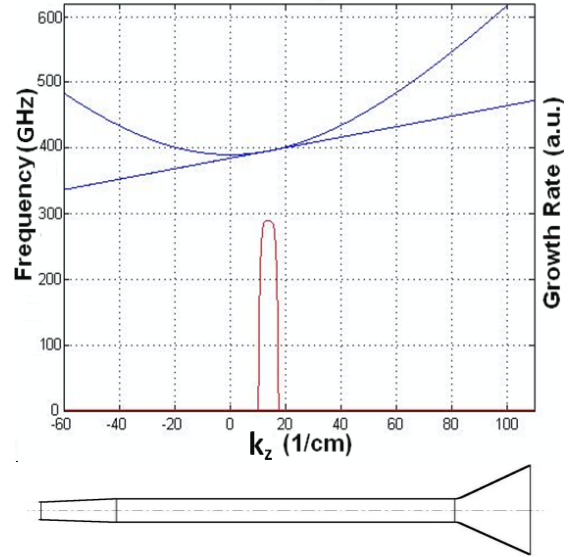


Figure 3. The growth rate at the 7th harmonic interaction (upper diagram) and the schematic gyrotron geometry (lower diagram).

The growth rate of this interaction can be obtained by solving the imaginary part of ω in equation (1) as a function of axial wavenumber k_z and is shown in figure 3. In the diagram the TE₇₁ cylindrical waveguide mode is interacting with the 7th harmonic of the electron cyclotron frequency of a beam with a velocity ratio α of 3 at a magnetic field of 2.09 T. The radius of the cylindrical cavity is 1.055 mm, and the cavity length is 50 mm at a reasonable cavity Q of 2000.

The cavity length L and the output taper angle are optimized for a reasonably high Q which is a very important parameter in any gyrotron design. The total Q of the resonant cavity is given by

$$\frac{1}{Q} = \frac{1}{Q_d} + \frac{1}{Q_{\Omega}} \quad (2)$$

The diffraction quality factor Q_d and the ohmic quality factor Q_{Ω} which are caused by diffraction and ohmic losses respectively, can be calculated using the equations below:

$$Q_d = 4\pi \frac{(L/\lambda)^2}{1 - |R_1 R_2|} \quad (3)$$

$$\frac{1}{Q_{\Omega}} = \left(\frac{\delta}{r_w} \right) \left[\frac{c^2}{\omega^2} \frac{x_{mn}^2}{r_w^2} + \left(\frac{x_{mn}^2}{x_{mn}^2 - m^2} \right) \right] \quad (4)$$

Where $\delta = \sqrt{\frac{2}{\omega\mu\sigma}}$ is the skin depth of the cavity wall,

σ is the conductivity of the cavity material, μ is the absolute permeability. R_1 and R_2 are the reflection coefficients at both ends of the cavity interaction region.

The cavity Q was calculated using the code Cascade [23]. In figure 4(a) the curve shows the simulated cavity Q as a function of the output taper angle at 390 GHz. In this diagram, the cavity was a 40 mm long smooth cylindrical cavity with a radius of $r_w = 1.055$

mm. The output taper was 10 mm in length and the input section of the cut-off taper had a fixed radius of 0.8 mm and a length of 20 mm. Though in a real situation the tolerance of the cavity dimensions, roughness of the cavity surface [24] and the purity of the materials will affect the value of the ohmic losses at high frequencies, the ideal surfaces and oxygen free high conductivity copper were applied to these calculations. From the diagram we can see the cavity Q increases as the angle increases, but in order to sustain enough output power and to decrease the heat load of the cavity [25], the taper angle needs to be properly selected. Considering all of these factors a 6 degree output taper was chosen in the cavity design. The cut-off taper angle was also studied by changing the length of the taper with a fixed cut-off input radius 0.8 mm. Cascade simulations show that these changes do not affect the cavity Q value very much (less than 20 when the cut-off taper length was varied from 5 mm to 20 mm).

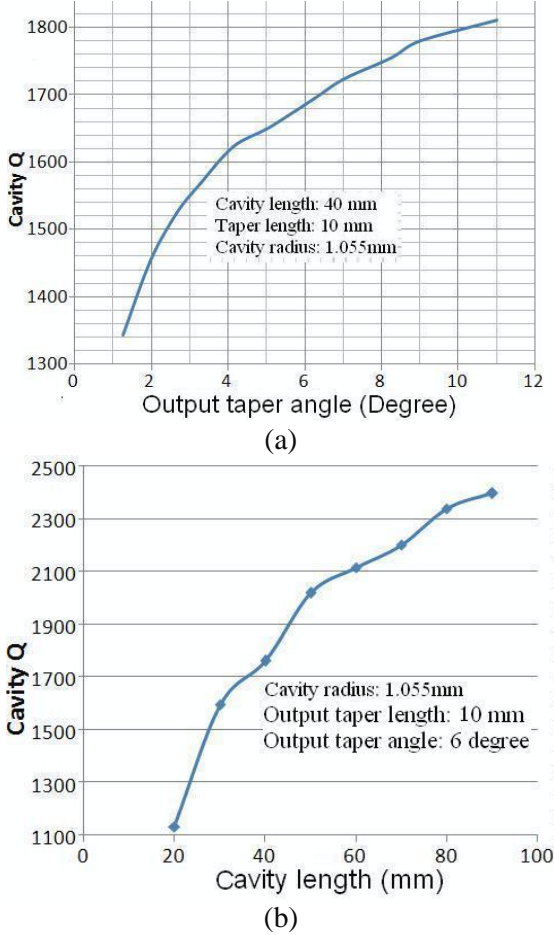


Figure 4. (a) Cavity Q as a function of output taper angle and (b) Cavity Q as a function of cavity length

Figure 4(b) shows the simulated cavity Q as a function of cavity length using the code Cascade. In the simulation the input end had a 20 mm taper with an input radius of 0.8 mm. The cavity radius remains the same as before which was 1.055 mm and at the end it had a 6 degree output taper. **Simulations using CST Microwave studio showed that there is no significant mode conversion (<10% of power) for this output taper**

at the operating mode. However, further increase of the output taper length or output taper angle will cause significant mode conversion. For example, when the taper length was increased to 20 mm, 70% of the power was converted to the TM_{52} mode.

The starting oscillation currents for this cavity at the design mode and competing modes can be calculated by using the equation shown below [12]:

$$I_s = \left(\frac{I_A}{Q}\right) \left(\frac{\omega}{s\Omega}\right) \left(\frac{\gamma L r_w^2 \omega k_z^2 \beta_z^2}{16c}\right) \left(1 - \frac{m^2}{x_{mn}^2}\right) \times \left(\frac{J_m(x_{mn})}{J'_m(x_{mn} \beta_{\perp} c / r_w \Omega)}\right)^2 R(X)^{-1} \quad (5)$$

Where:

$$R(X) = \left\{2 - 2x \left(\frac{\beta_{\perp}^2}{\beta_z}\right) \left(\frac{k_z c}{s\Omega}\right) + \left[\left(\frac{r_w s\Omega}{\beta_{\perp} c x_{mn}}\right)^2 - 1\right] \left(\frac{J_n(x_{mn} \beta_{\perp} c / r_w \Omega)}{J'_n(x_{mn} \beta_{\perp} c / r_w \Omega)}\right)^2 + \left(\frac{2x_{mn} \beta_{\perp} c}{r_w \Omega}\right) \left(\frac{J_n''(x_{mn} \beta_{\perp} c / r_w \Omega)}{J'_n(x_{mn} \beta_{\perp} c / r_w \Omega)}\right)\right\} G(X) + \left(\frac{\beta_{\perp}^2}{\beta_z}\right) \left(\frac{\omega}{s\Omega}\right) \left[\frac{\omega}{ck_z} - \left(\frac{ck_z}{\omega}\right) X^2\right] G'(X) \quad (6)$$

and: $X = (\omega - s\Omega) / k_z \beta_z c$,

$$G(X) = \begin{cases} [\cos(\pi q X / 2) / (1 - X^2)]^2 & \text{(odd } q) \\ [\sin(\pi q X / 2) / (1 - X^2)]^2 & \text{(even } q) \end{cases} \quad (7)$$

Here $q = k_z L / \pi$, and the calculation result is shown in figure.5. In this calculation the cavity $Q = 2000$, and the electron beam velocity ratio α was 3.

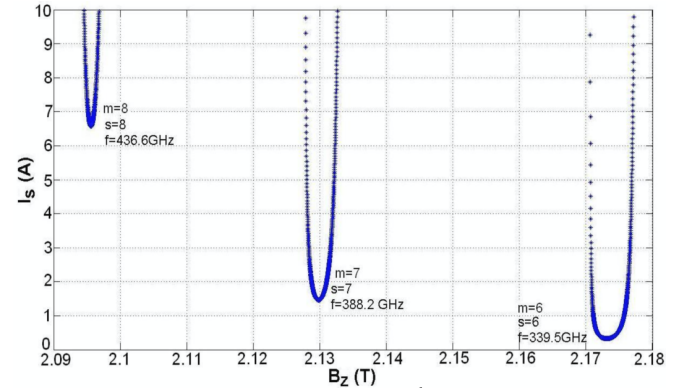


Figure 5. Starting currents for the 7th harmonic TE_{71} mode and its neighboring TE_{m1} modes.

The minimum starting current for the 7th harmonic mode is 1.4 A, at a magnetic field of 2.13 T which are both within the capability of our cusp gun design current of 1.5-1.7 A and the solenoid magnetic field of 2.16 T. This diagram shows clearly that the neighboring modes $s = 8$ and $s = 6$ will be eliminated as the starting current for the 8th harmonic requires a starting current of more than 6 A, and the magnetic field requirement for the 6th harmonic is above 2.17 T.

4. Simulation results

In order to demonstrate the beam-wave interaction can take place in the designed gyrotron cavity, the code MAGIC was used to simulate the harmonic gyrotron interaction. The R-Z plane geometries of the smooth cylindrical structures and electron trajectories are shown in figure. 6. An ideal beam with the parameters

from the cusp electron simulation but without velocity and radius spreads was emitted from the left end of the cavity and propagated in a uniform B-field produced by a solenoid in the magic simulation. The right end of the solenoid sits in the middle of the output taper in the Z axis. During the simulation, the cavity length was reduced from 50 mm to 30 mm as the cavity ohmic loss was neglected in the simulation. A schematic diagram of the simulation is shown in figure 6 with the magnetic field profile produced by the solenoid.

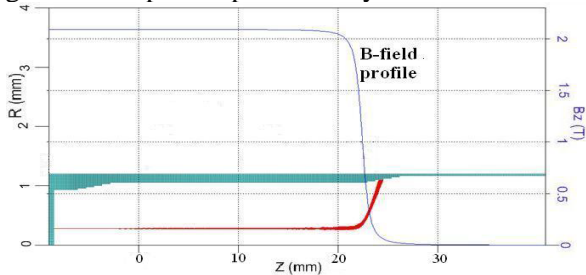


Figure 6. A Schematic diagram of gyrotron in the R-Z plane with simulated electron beam trajectories.

The simulation result is shown in figure 7. In the simulation the large orbit annular electron beam had a voltage of 40 kV, current of 1.5 A with a beam velocity ratio α of 3. The magnetic B-field applied in the cavity was 2.09 T. The magnetic field difference between the MAGIC and analytical calculation is due to the grid density in the gyrotron simulation, when a higher grid density is used, the B-field required in the simulation will be larger and closer to the analytically calculated value.

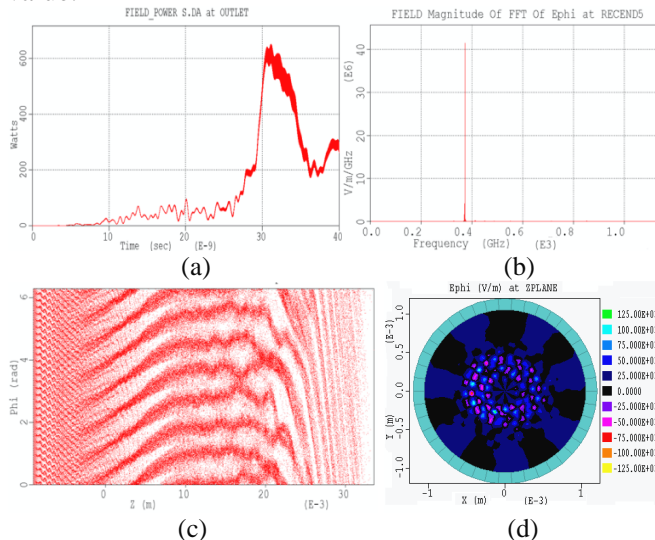


Figure 7. Simulation results of the 7th harmonic gyrotron with a smooth cavity: (a) output power, (b) output spectrum and (c) electron phase angle as a function of axial position (d) microwave E_ϕ field pattern at resonance.

The electron phase angle as a function of axial position Z (figure 7(c)) indicates the interaction occurred at the 7th harmonic of the electron cyclotron frequency. Very pure radiation output at a frequency of 384 GHz was observed in the simulation as shown in figure 7(b) and ~600 W of output power was achieved in this simulation. The reduction in power observed after ~30

ns arises due to the cavity of 30 mm length being sufficiently long in the absence of wall loss, for the interaction to enter phase trapped saturation resulting in re-absorption of the wave energy – these can be seen in figure 7(c) where the electron distribution in phase angle illustrates the trapping occurring. When 0.1 mm beam thickness and 25% beam spread were introduced in the simulation, it was found that the total output power dropped to ~500 W while a competing TE_{61} became slightly dominant at the output. The output power at the designed frequency and mode dropped to ~200 W.

5. Conclusion

In conclusion a ~390 GHz harmonic gyrotron based on a large orbit electron beam was designed and simulated. The cavity has been analyzed and optimized. Theoretical and numerical simulation results demonstrate that the beam interacts with the single TE_{71} mode and a simulated output power of ~600 W was achieved while using a 40 kV, 1.5 A, large orbit electron beam with velocity ratio α of 3. It was found from simulation that spread in α will cause the reduction of the output power and start-up of mode competition. The effect of beam parameters such as velocity spread, envelop ripple, might have on the starting current and mode excitation [26] will be studied both numerically and experimentally in the future.

Acknowledgments

The authors would like to thank the Faraday Partnership in High Power RF and the Scottish Universities Physics Alliance (SUPA) and Overseas Research Students Awards Scheme (ORSAS) for supporting this project. The authors would also like to thank “Calabazas Creek Research” for providing the 1 month free license for Cascade.

References

- [1] D. Wagner, F. Leuterer, A. Manini, et al., “The New Multi-Frequency Electron Cyclotron Resonance Heating System for ASDEX Upgrade,” *Fusion Sci. Tech.*, Vol. 52, No. 2, pp. 313-320. Aug. 2007.
- [2] T. Saito, Takashi Notake, Yoshinori Tatematsu, et al., “Development of a Sub Terahertz High Power Pulse Gyrotron for Collective Thomson Scattering,” presented at the Joint 33rd Int. Conf. Infrared Millimeter, 16th Int. Conf. Terahertz Electronics, Pasadena, CA, 2008, Paper ICIMW.2008.4665739.
- [3] P. Bhartia and I. J. Bahl, *Millimeter Wave Engineering and Applications*. New York: Wiley, 1984.

- [4] P. H. Siegel, "Terahertz Technology," *IEEE Trans. Microwave Theory Tech.*, vol. 50, no. 3, pp. 910-928, Mar. 2002.
- [5] D. Clery, "Brainstorming their way to an imaging revolution," *Sci.*, vol. 297, no. 5582, pp. 761-763, Aug. 2002.
- [6] A. C. Torrezen, S. T. Han, M. A. Shapiro, et al., "CW Operation of a Tunable 330/460 GHz Gyrotron for Enhanced Nuclear Magnetic Resonance," presented at the Joint 33rd Int. Conf. Infrared Millimeter, 16th Int. Conf. Terahertz Electronics, Pasadena, CA, 2008, Paper ICIMW.2008.4665733.
- [7] M. Yu, Glyavin, A. G. Luchinin, and G. Yu. Golubiantnikov, "Generation of 1.5-kW 1-Thz Coherent radiation from a gyrotron with a pulsed magnetic field," *Phys. Rev. Lett.*, vol. 100, no. 1, 015101, Jan. 2008.
- [8] T. Idehara, I. Ogawa, S. Mitsudo, Y. Iwata, et al., "A high harmonic Gyrotron with an axis-encircling electron beam and a permanent magnet," *IEEE Trans. Plasma. Sci.*, vol. 32, no. 3, pp. 903-909, Jun. 2004.
- [9] Q. S. Wang, D. B. McDermott, C. K. Chong, C. S. Kou, et al., "Stable 1 MW, third-harmonic Gyro-TWT Amplifier," *IEEE Trans. Plasma. Sci.*, vol. 22, no. 5, pp. 608-615, Oct. 1994.
- [10] Q. S. Wang, H. E. Huey, D. B. McDermott, et al., "Design of a W-Band Second-Harmonic TE₀₂ Gyro-TWT Amplifier," *IEEE Trans. Plasma Sci.*, vol. 28, no. 6, pp. 2232-2237, Dec. 2000.
- [11] La Agusu, H. Murase, T. Idehara, etc., "Design of a 400 GHz Gyrotron for DNP-NMR Spectroscopy," presented at the Joint 31st Int. Conf. Infrared Millimeter, 14th Int. Conf. Terahertz Electronics, Shanghai, China, 2006, Paper ICIMW.2006.368290.
- [12] D. B. McDermott, N. C. Luhmann, Jr., A. Kupisedwski, and H. R. Jory, "Small-signal theory of a large-orbit electron-cyclotron harmonic maser," *Phys. Fluids*, vol. 26, no. 7, pp. 1936-1941, Jul. 1983.
- [13] G. Schmidt, "Nonadiabatic Particle Motion in Axiallysymmetric Fields," *Phys. Fluids*, vol. 5, no. 8, pp. 994-1002, Aug. 1962.
- [14] W. He, C. R. Donaldson, A. D. R. Phelps, A. W. Cross, et al., "A W-band Gyro-BWO based on a Helically Corrugated Waveguide," Infrared Millimeter Waves and 14th International Conference on Terahertz Electronics, 2006, Joint 31st International Conference on IRMMW-THz 2006, pp.88-88, Sep, 2006.
- [15] W. He, C. G. Whyte, E. G. Rafferty, A. W. Cross, et al., "Axis-encircling electron beam generation using a smooth magnetic cusp for gyro-devices," *Appl. Phys. Lett.*, vol. 93, no. 12, 121501, Sep. 2008.
- [16] V. L. Bratman, Yu. K. Kalynov, V. N. Manuilov, et al., "Submillimeter-wave large-orbit Gyrotron," *Radiophysics and Quantum Electronics*, vol. 48, No. 10-11, pp. 731-736, Oct. 2005.
- [17] V. L. Bratman, Yu. K. Kalynov, and V. N. Manuilov, "Large-orbit Gyrotron Operation in the Terahertz Frequency Range," *Phys. Rev. Lett.*, vol. 102, no. 24, 245101, Jun. 2009.
- [18] W. He, C. R. Donaldson, F. Li, A. W. Cross, et al., "Design, Simulation and Experiment of a Cusp Electron Beam for Millimeter Wave Gyro-devices," IVEC, Rome, Italy, 2009.
- [19] C. R. Donaldson, W. He, A. W. Cross, et al., "Design and Numerical Optimization of a Cusp-Gun-Based Electron Beam for Millimeter-Wave Gyro-Devices," *IEEE Trans. Plasma Sci.*, vol. 37, no. 11, pp. 2153-2157, Oct. 2009.
- [20] K. R. Chu, "The electron cyclotron maser," *Rev. Mod. Phys.*, vol. 76, no. 2, pp. 486-540, Apr. 2004.
- [21] K. R. Chu, and Anthony T. Lin, "Gain and Bandwidth of the gyro-TWT and CARM Amplifiers," *IEEE Trans. Plasma Sci.*, vol. 16, no. 2, pp. 90-104, Apr. 1988.
- [22] D. S. Furuno, D. B. McDermott, C. S. Kou, et al., "Operation of a Large-Orbit High-Harmonic Gyro-Traveling-Wave Tube Amplifier," *IEEE Trans. Plasma Sci.*, vol. 18, no. pp. 313-320, Jun. 1990.
- [23] L. Ives, J. Nelson and W. Vogler, "Cascade-An advanced computational tool for waveguide components and window design," Proceedings of the 2003 Particle Accelerator Conference, Portland, USA, 2003.
- [24] T. S. Thorpe, "RF Conductivity in Copper at 8 mm Wavelengths," *Proc. Inst. Elec. Eng.*, vol.101, Pt. III, pp. 357-359, 1954,
- [25] V. E. Zapevalov, Yu. K. Kalynov, A. N. Kuftin, et al., "Low-Q cavities for high-power gyrotrons," *Radiophysics and Quantum Electronics*, vol. 37, no. 3, pp. 233-236, Mar. 1994.
- [26] V. L. Bratman, Yu. K. Kalynov and A. E. Fedotov, "Theory of gyro devices with thin electron beams (large-orbit gyrotron)," *Technical Physics*, vol. 43, no. 10, pp. 1219-1225, Oct. 1998.